NASA TECHNICAL NOTE

NASA TN D-3788

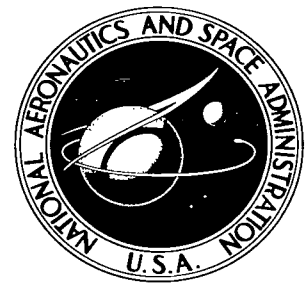

NASA TN D-3788

COMPARISON OF SOLAR DIRECT-ENERGY CONVERSION SYSTEMS OPERATING BETWEEN 1.0 AND 0.1 ASTRONOMICAL UNIT

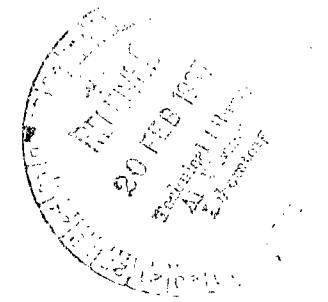

by William J. Bifano and Larry R. Scudder

Lewis Research Center
Cleveland, Ohio

NATIONAL AERONAUTICS AND SPACE ADMINISTRATION • WASHINGTON, D. C. • FEBRUARY 1967

NASA TN D-3788

COMPARISON OF SOLAR DIRECT-ENERGY CONVERSION SYSTEMS OPERATING BETWEEN 1.0 AND 0.1 ASTRONOMICAL UNIT

By William J. Bifano and Larry R. Scudder

Lewis Research Center
Cleveland, Ohio

NATIONAL AERONAUTICS AND SPACE ADMINISTRATION

For sale by the Clearinghouse for Federal Scientific and Technical Information
Springfield, Virginia 22151 – Price $2.00

COMPARISON OF SOLAR DIRECT-ENERGY CONVERSION SYSTEMS OPERATING BETWEEN 1.0 AND 0.1 ASTRONOMICAL UNIT

by William J. Bifano and Larry R. Scudder

Lewis Research Center

SUMMARY

Three solar direct-energy conversion systems for operation in the 1.0 to 0.1 AU range were compared: thermoelectric flat plates (employing either lead telluride or silicon-germanium semiconductors), thermionic systems (including the solar concentrator), and uncooled silicon solar cells. System specific weight and power output variation during flight were used as a basis of comparison by assuming that an output power of 200 watts was required at the design point. Tilting the thermoelectric and solar cell panels from 0^{o} (panel normal to the incident radiation) to 80^{o} was assumed a means of solar flux control; however, no solar flux control was assumed for the thermionic systems.

The results indicate that silicon solar cells provide relatively constant output power from 1.0 to about 0.2 AU. Between 0.2 and 0.15 AU, the output power decreases rapidly to zero because of excessive cell operating temperatures. Solar thermoelectric flat plates and thermionic systems have potential application to within 0.1 AU or less; however, their electrical output power between 1.0 AU and the design point is initially low, increasing rapidly as the design point is approached. The results thus indicate that a hybrid system incorporating solar cells and perhaps a thermoelectric flat plate would provide a continuous power output from Earth to 0.1 AU.

INTRODUCTION

For missions directed toward the Sun, the abundance of available solar energy suggests that a solar direct-energy conversion system be used to provide auxiliary electrical power. Direct-energy conversion devices could satisfy the need for a lightweight reliable power supply capable of producing power for a long period of time (approximately 1 yr for a solar probe). However, the use of these systems presents a thermal control problem because of the large variation in solar intensity encountered during flight. For example, the average solar flux, 130 watts per square foot (1400 W/sq m) at 1.0 AU, increases by factors of 6.7 and 100 at 0.388 (Mercury) and 0.1 AU, respectively. (An astronomical unit AU is defined as the mean Earth-Sun distance.)

This study considers three solar direct-energy conversion systems, which may be

employed in the 1.0 to 0.1 AU region: thermoelectric flat plates (utilizing either lead telluride or silicon-germanium semiconductors), thermionic systems, and photovoltaic systems (silicon solar cells). The thermoelectric and thermionic systems are sized to produce 200 watts of electrical power with a minimum weight at the following design points: 1.0 AU (Earth), 0.722 AU (Venus), 0.388 AU (Mercury), 0.25 AU, and 0.1 AU. Each design point requires a unique design geometry for the thermoelectric and thermionic systems because of optimum thermal balance considerations. The photovoltaic panel is designed to produce a maximum of 200 watts in the 1.0 to 0.1 AU range assuming a fixed solar cell geometry. Tilting was the only means of solar-flux control employed for both the thermoelectric flat plate and the solar cell array, whereas no solar-flux control was provided for the thermionic system. (Solar flux controls required for the thermionic systems studied herein have not yet been developed.)

Although it is theoretically possible to tilt the panels to any given angle, the accuracy required of the orientation system will place a practical limit on the maximum usable tilt angle. This results because the effect of an error in orientation becomes more pronounced as the angle of tilt increases; these errors in orientation result in either overheating of the panels (excessive incident solar flux) or a rapid decrease in the power output (insufficient incident solar flux), dependent on the direction of the orientation error. For this study, the maximum tilt angle was chosen to be 80° to illustrate the effect of this limitation. However, this choice does not affect the comparisons of system performance presented herein.

System specific weight given in pounds (and kg) per electrical kilowatt (excluding auxiliary equipment such as dc-dc power conversion systems, orientation controls, and vehicle attachments) and power output variation during flight are used as a basis for comparison. In addition to the power profiles presented for the three 200-watt systems, the thermoelectric flat plate is compared with solar cell panels on the basis of electrical power generated per square foot of panel.

METHOD OF ANALYSIS FOR FLAT-PLATE THERMOELECTRIC SYSTEM

General System Description

A schematic diagram of a unit thermoelectric couple is shown in figure 1(a). In general, the couple consists of an n-type and a p-type semiconductor element directly joined at one end (hot junction). Waste heat is rejected at the cold junction and useful power is obtained by placing a load between the p and n legs.

Figure 1(b) illustrates one of several possible thermoelectric flat-plate designs in which thermoelements are sandwiched between absorber and radiator plates. A selective coating is applied to the absorber to obtain the proper solar absorptance and thermal emittance and to the radiator to obtain a high thermal emittance.

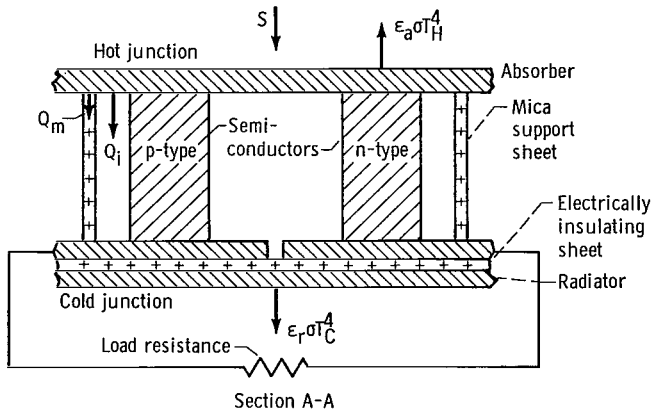

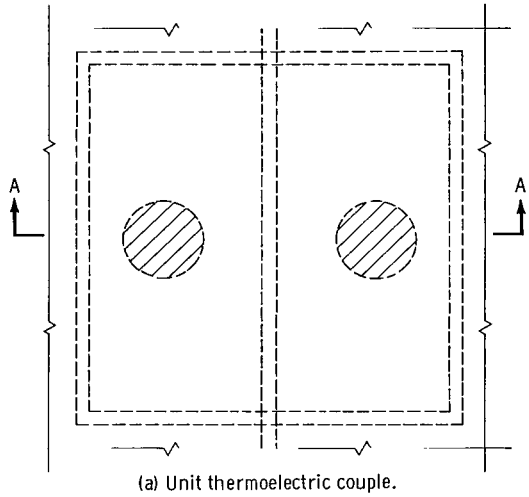

(a) Unit thermoelectric couple.

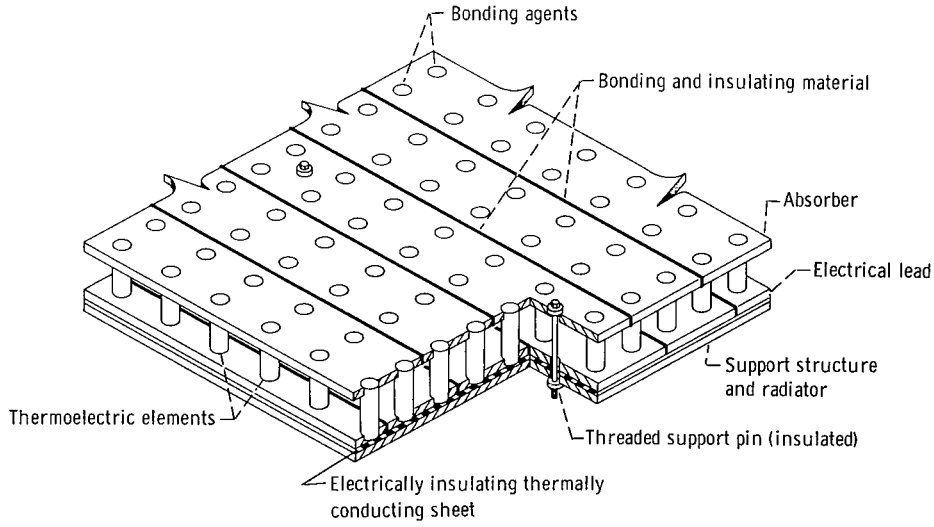

(b) Isometric view.

Figure 1. - Flat-plate thermoelectric system.

The function of a solar absorber coating is to absorb a large fraction of the incident solar radiation (predominantly in the 0.2- to 2.0-μ wavelength range) and to reradiate as little energy as possible. In general, coatings with a high ratio of solar absorptance to thermal emittance (α_a/ϵ_a) were chosen for this study (on the order of 10 to 12). (Symbols are defined in appendix A.) Although coatings are available having the desired (α_a/ϵ_a) ratio, these coatings have not demonstrated as yet long-term stability at high operating temperatures.

Each couple is surrounded by four thin support sheets (fig. 1(a)). Ribbed supports are provided on the radiator plate to improve the structural rigidity of the panel, and an insulating sheet is employed to electrically isolate the elements from the radiator. Interplate heat loss is minimized by either applying low-emittance radiative-barrier coatings to the inner surfaces of the plates or by using solid thermal insulation between the plates. The choice is dependent on operating temperatures.

Thermal Analysis and Optimization

For a given design point, system performance is determined over a range of hot-junction temperatures by using a heat balance approach, and the design with the maximum output power density is selected as the optimized system. Maximum operating temperatures are taken to be 1000° F (811° K) for lead telluride and 1800° F (1255° K) for silicon-germanium. The performance of the bonded thermoelectric material is discussed in appendix B. The selective absorber coating compatible with the assumed substrate material and having the proper solar absorptance and thermal emittance characteristics is employed.

For a given mission and assumed hot-junction temperature T_H, the net thermal power input to the absorber is found by using the following equation:

$$\frac{Q}{A_s} = \alpha S - \epsilon_a \sigma T_H^4 \tag{1}$$

The cold-junction temperature is found by using the following equation:

$$T_C = \left[\frac{\frac{Q}{A_s}(1 - \eta_d)}{\epsilon_r \sigma} \right]^{1/4} \tag{2}$$

Since equations (1) and (2) do not include the effect of temperature variations along

the panel surface, fin effectiveness calculations were made by using the approach employed in reference 1. (The fin effectiveness represents the fraction of heat radiated from a plate having a maximum temperature T relative to a plate at a uniform temperature T.) For all design points considered in this study, calculated fin effectiveness was 0.92 or greater. Since values of fin effectiveness greater than 0.9 result in only slight changes in system performance, the simplifying assumption of a fin effectiveness of 1.0 was employed throughout the study.

For given hot- and cold-junction temperatures, the actual device efficiency and power density are determined by using the device performance curves given in appendix B. (The term "device" refers to the bonded thermoelectric material only and must be distinguished from the term "system.") The cold-junction temperature determined with $\eta_d = 0$ (eq. (2)) was found adequate for the analysis, and iteration was unnecessary. For example, when $\eta_d = 6.0$ percent, the use of $\eta_d = 0$ results in a 1 percent error in T_C.

The thermoelectric cross-sectional area coverage required A_c/A_s is found by using the following equation:

$$\frac{A_c}{A_s} = \frac{\frac{Q}{A_s} - \frac{Q_m + Q_i}{A_s}}{\frac{P/A_c}{\eta_d}} \tag{3}$$

Iteration is required in solving equation (3) since the thermal loss through the support sheets Q_m is dependent on the ratio of thermoelectric cross-sectional area to plate area A_c/A_s. The product of the thermoelectric device power density P/A_c and the area coverage ratio A_c/A_s is then taken as the generator output power density:

$$\frac{P}{A_s} = \frac{P}{A_c}\frac{A_c}{A_s} \tag{4}$$

The procedure is then repeated with new assumed hot-junction temperatures until a maximum value of output power density is found. The variation in output power density with Sun-power system distance (power profile) is then calculated for each configuration by using equations (1) to (4). Constant thermal power input is maintained as the system moves from design point toward the sun by assuming that the panel is tilted through

angles up to 80°. The variation of solar absorptance with tilt angle is neglected in this analysis.

Specific Weight

The following components are considered in calculating panel specific weight (i.e., the ratio of generator weight to output power, lb/kWe): (1) semiconductor elements, (2) electrical interconnections, (3) absorber and radiator plates, (4) interplate thermal insulation (when necessary), (5) insulating support sheets, and (6) ribbed support structure. The sum of the element, lead, plate, and support-sheet weights is taken as the weight of the support structure. The structure would include ribs or other stiffeners applied to the panel.

The materials used for the various systems are discussed in appendix B, and their physical properties are listed in table I.

System Performance

Design parameters and system performance values are summarized in table I. Panel output power density is plotted against distance from the Sun in figure 2 for 0.1-, 0.25-, and 0.388-AU missions. As shown in figure 2, for a given mission design point, panel output power density P/A_s exhibits a slow increase initially with decreasing distance from the Sun followed by a sharp increase as the system nears design point. For example, a lead telluride system designed for 0.388 AU exhibits an output power density, which increases from about 1 watt per square foot (10.77 W/sq m) at 1.0 AU to 13 watts per square foot (140 W/sq m) at 0.388 AU and then remains constant with the assumption of continuous tilting to about 0.16 AU where the limiting tilt angle of 80° is attained. Although lead telluride was also considered for 0.722- and 1.0-AU missions, the power densities of these systems were relatively low and are not presented in the figures.

A silicon-germanium flat plate designed for 0.388 AU exhibits a variation in output power relative to position in space similar to the lead telluride system but with a slightly higher power density of 17 watts per square foot (183 W/sq m) at design point. The silicon-germanium systems designed for 0.25 and 0.1 AU are of special interest because of their possible use in solar probe missions. As shown in figure 2, the 0.25-AU system exhibits a power density increase from 14 watts per square foot (151 W/sq m) at 0.388 AU, to 49 watts per square foot (528 W/sq m) at 0.25 AU and then remains constant to about 0.1 AU where the required tilt angle is 80°. The 0.1-AU system power density variation is similar, increasing from 1 watt per square foot (10.77 W/sq m) at 0.388 AU

TABLE I. - THERMOELECTRIC PANEL MATERIAL PROPERTIES AND CALCULATED VALUES OF SYSTEM PERFORMANCE

[Radiator coating, calcium titanate; thermal insulating supports, mica; density of thermal insulating supports, 0.1154 lb/cu in. (3.19 g/cu cm).]

Properties	Semiconductor					
	Lead telluride			Silicon germanium		
	Design point					
	Earth	Venus	Mercury	Mercury	----	----
	Distance from Sun, AU					
	1.0	0.722	0.388	0.388	0.25	0.10
Solar constant, W/sq ft (W/sq m)	130 (1400)	248 (2670)	865 (9310)	865 (9310)	2075 (22 350)	13 000 (140 000)
Solar absorptance, α_a	[a].90	[a].90	.86	.85	[b].85	.36
Emittance						
Absorber plate, ϵ_a	[a].05	[a].05	.22	.072	[b].072	.15
Radiator plate, ϵ_r	.90	.90	.90	.90	.90	.90
Temperature, ^{o}F (^{o}K)						
Hot junction, T_H	700 (644)	800 (700)	1000 (811)	1200 (922)	1600 (1144)	1800 (1255)
Cold junction, T_C	168 (349)	306 (425)	400 (477)	540 (555)	785 (691)	1098 (865)
Difference, ΔT	532 (295)	494 (275)	600 (334)	660 (367)	815 (453)	702 (390)
Net thermal input to absorber, Q/As, W/sq ft (W/sq m)	71 (765)	158 (1700)	249 (2680)	457 (4920)	1103 (11 900)	2690 (29 000)
Ratio of thermoelectric element, cross-sectional area to plate area, Ac/As	.0046	.0124	.0179	.012	.0237	.0698
Device power density, P/Ac, W/sq ft (W/sq m)	710 (7650)	638 (6880)	750 (8070)	1415 (15 240)	2090 (22 500)	1480 (15 900)
Generator output power density, W/sq ft (W/sq m)	3.3 (35.5)	7.9 (85)	13.4 (144)	17.0 (183)	49.5 (533)	103.8 (1120)
Efficiency, percent						
Device, η_d	5.87	5.76	6.35	4.20	5.13	4.30
Overall, η_o	2.53	3.18	1.55	1.97	2.38	.80
Innerplate surface emittance, ϵ_p	.03	.03	.03	.03	.03	None
Panel specific weight, lb/kWe (kg/kWe)	117.0 (53.2)	97.5 (44.3)	73.6 (33.4)	82.4 (37.4)	30.8 (14.0)	31.6 (14.35)
	Absorber plate					
	Copper			Molybdenum		
Density, lb/cu in. (g/cu cm)	0.322 (8.89)	0.322 (8.89)	0.322 (8.89)	0.370 (10.2)	0.370 (10.2)	0.370 (10.2)
Thickness, in. (mm)	.002 (0.0508)	.004 (0.102)	.005 (0.127)	.005 (0.127)	.005 (0.127)	.005 (0.127)
	Radiator plate					
	Aluminum			Molybdenum		
Density, lb/cu in. (g/cu cm)	0.098 (2.71)	0.098 (2.71)	0.098 (2.71)	0.370 (10.2)	0.370 (10.2)	0.370 (10.2)
Thickness, in. (mm)	.003 (0.0762)	.005 (0.127)	.005 (0.127)	.005 (0.127)	.005 (0.127)	.005 (0.127)
	Absorber coating					
	Hass dark mirror		Tabor chemical treatment 110-30	Optical interference coating (MgF_2-Mo-CeO_2)		Polished molybdenum
	Innerplate radiation barrier coating					
	Gold			Gold		None
	Interplate thermal insulation					
	None			None		Min-K 200
Density, lb/cu in. (g/cu cm)	----			----		0.011 (0.304)

[a]Represent projected values; however, coating has demonstrated $\alpha_a > 0.8$ and $\epsilon_a < 0.07$.

[b]Represent measured values at 1250° F (projected to 1600° F).

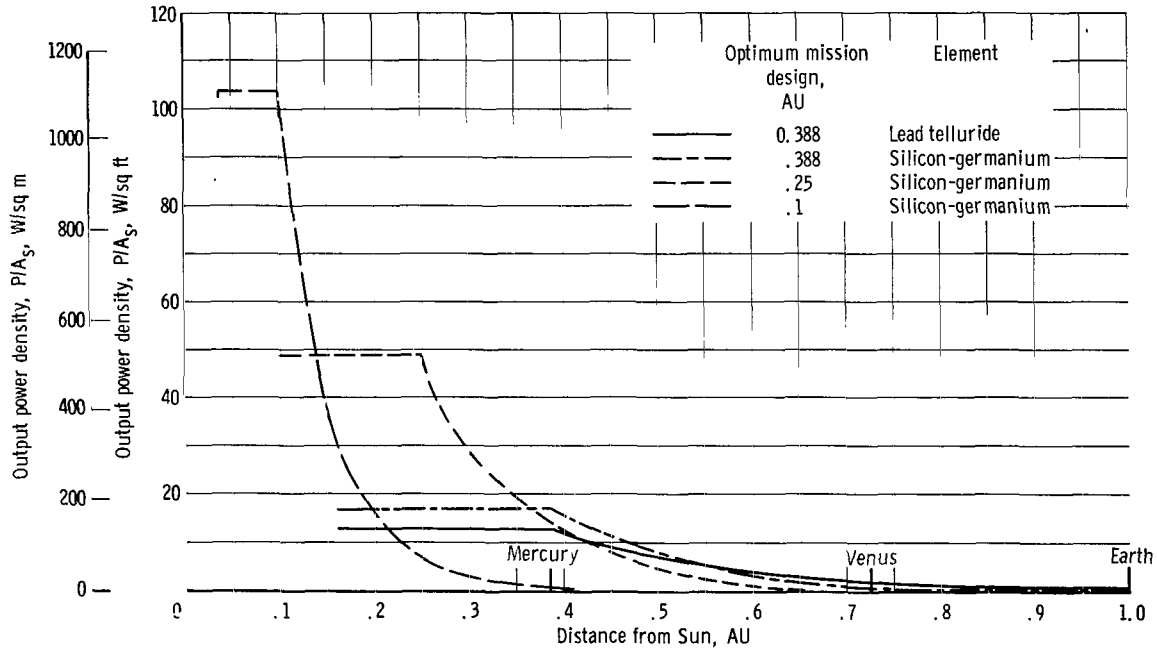

Figure 2. - Power density profiles for solar thermoelectric flat-plate systems optimized for 0.1, 0.25, and 0.388 AU missions.

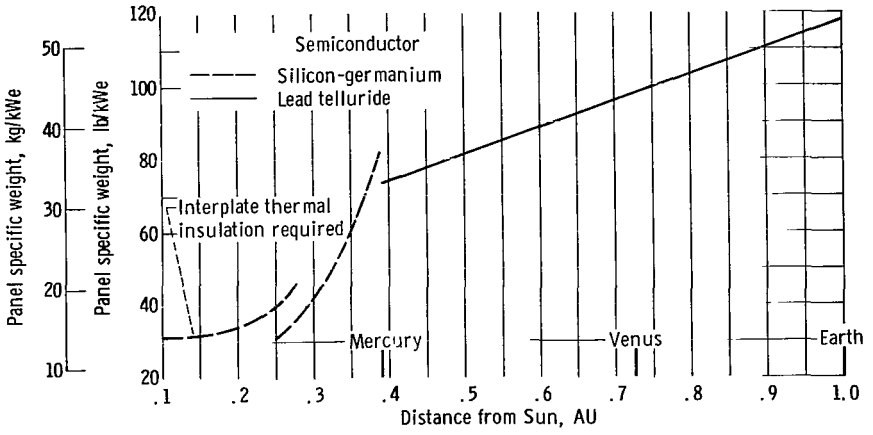

Figure 3. - Panel specific weight plotted against design-point distance from Sun for flat-plate thermoelectric generator.

to 104 watts per square foot (1120 W/sq m) at 0.1 AU. Again, tilting of the panels is assumed to maintain constant output power density to 0.04 AU, where the limiting tilt angle of 80° is reached.

Panel specific weight at design point is plotted against distance from the Sun in figure 3. For a given distance from the Sun, the specific weight shown in figure 3 represents that of a system designed to produce maximum output power density at that distance with the panels oriented normal to the rays of the Sun (i.e., a tilt angle of 0°). For lead telluride, the design point specific weight decreases steadily from 1 to 0.388 AU where the hot-junction temperature reaches 1000° F (811° K) (the limiting temperature for lead telluride). For silicon-germanium, the design point specific weight decreases sharply between 0.388 and 0.25 AU for the panels without interplate thermal insulation, while a more gradual decrease is exhibited between 0.25 and 0.1 AU when interplate thermal insulation is employed. Low-emittance radiative-barrier coatings for minimizing the thermal loss between the absorber and radiator plates are assumed to be usable only up to 1600° F (1144° K). Therefore, for design points less than 0.25 AU, corresponding to absorber temperatures in excess of 1600° F (1144° K), solid thermal insulation is required between the plates.

As shown in figure 3, the specific weight of the lead telluride panels varies from 118 pounds per kilowatt electric (53.5 kg/kWe) at 1.0 AU to about 74 pounds per kilowatt electric (33.6 kg/kWe) at 0.388 AU, while that of the silicon germanium panels varies from 82 pounds per kilowatt electric (37.3 kg/kWe) at 0.388 AU to 31 pounds per kilowatt electric (14.1 kg/kWe) at 0.25 AU without interplate thermal insulation and from 40 pounds per kilowatt electric (18.2 kg/kWe) at 0.25 AU to 31 pounds per kilowatt electric (14.1 kg/kWe) at 0.1 AU when interplate insulation is included.

METHOD OF ANALYSIS FOR THERMIONIC SYSTEM

General System Description

A cross-sectional view of a typical planar cesium vapor diode is shown in figure 4(a). Four such conversion devices mounted on the outer walls of a solar absorber (fig. 4(b)) constitute the solar thermionic generator assumed for this study. In application, solar energy is directed through the aperture into the absorber by a one-piece parabolic mirror or concentrator (fig. 4(c)). A portion of this input is lost by thermal reradiation and reflection from the aperture and by conduction and radiation to the outer walls of the generator. The remainder is the thermal input to the emitting electrodes of the thermionic converters. Based on the diode performance assumed for this study, a maximum of approximately 15 percent of this thermal input is converted to electricity, while the remaining 85 percent or more is rejected to space by the diode radiator.

The concentrator and generator are connected by support arms (fig. 4(c)) such that the aperture, located on the front side of the generator, is in the focal plane of the concentrator. The outer walls of the generator are covered with a sufficient amount of thin-foil thermal-radiation shielding (fig. 4(b)), to limit the thermal loss from the generator to 10 percent of the net thermal input power.

Thermal Analysis and Optimization

In order to determine overall system performance, the following procedure is used: (1) For each design point, the generator is designed to produce a maximum of 200 watts of electrical output power (i.e., each of four planar diodes is sized to produce 50 watts of electrical power at design point when operating at an emitter temperature of 2050° K). (2) The solar concentrator is designed to deliver the net thermal input required by the generator and also to withstand the maximum operating temperatures reached during the mission. Two modes of diode control are assumed in determining system performance. The first involves continuous adjustment of the cesium reservoir temperature T_{Cs} and load resistance R_L to obtain maximum diode power density, referred to as "continuous diode control." The second involves control of T_{Cs} and R_L at fixed optimum values corresponding to an emitter temperature of 2050° K, referred to as "fixed diode control."

The total emitter area in square centimeters required to produce 200 watts of electrical power at an emitter temperature of 2050° K is determined from the following relation:

$$A_E = \frac{200}{p_{(2050^\circ\ K)}}$$

where p is the thermionic power density in watts per square centimeter. (See appendix C for thermionic power density and efficiency as functions of emitter temperature.)

For each design point, the solar collector size necessary to deliver the required thermal flux is determined. The variation in output power with distance from the Sun is then found by allowing the input thermal flux to the diodes to vary at the same rate as the incident solar flux with distance from the Sun (i.e., inverse square relation). The thermal power density required by the thermionic diodes is the ratio of electrical power density to efficiency. For a given decrease in thermal flux, the corresponding change in electrical power density is found by using the diode performance curves given in appendix C.

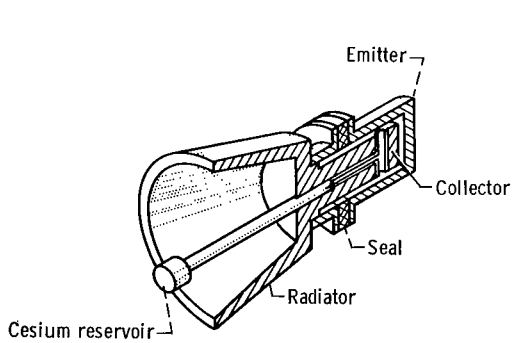

(a) Converter.

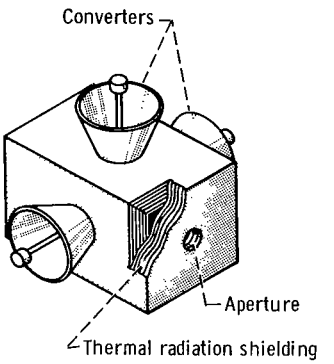

(b) Generator.

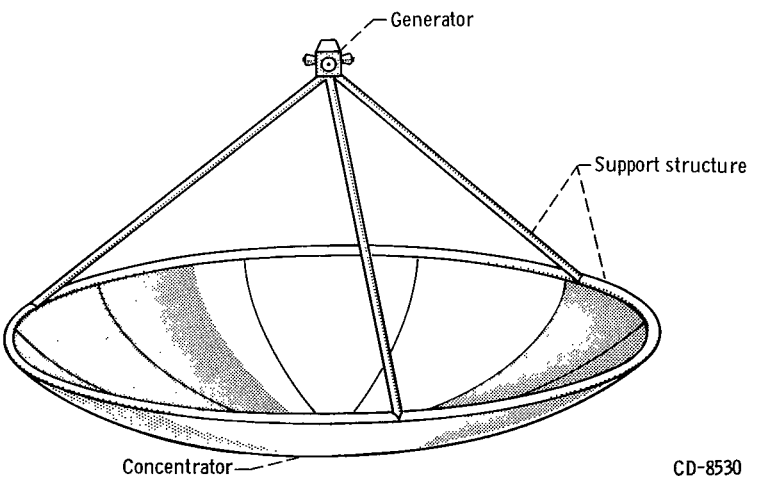

(c) Overall view.

Figure 4. - Solar thermionic conversion system.

Specific Weight

The system specific weight in pounds (and kg) per electrical kilowatt is calculated for each design point assuming the following components: solar concentrator, generator (including thermionic converters and thermal shielding), and generator supports. A detailed discussion of component weight is given in appendix C.

System Performance

In figure 5 electrical output power is given as a function of distance from the Sun for a 200-watt system for 0.1-, 0.25-, 0.388-, and 0.722-AU missions. For a given mission, output power increases sharply with decreasing distance from the Sun for both the continuous and fixed diode control conditions. The useful range of operation could be extended beyond the design point by using, for example, a shutter-type solar-flux control system. However, since the effectiveness of such controls has not been established for the missions evaluated in this analysis, performance predictions are made with the assumption of no solar-flux control.

For a 0.1-AU mission, a solar thermionic system employing continuous diode control does not begin to produce electrical power until the system reaches about 0.25 AU (see fig. 5). From 0.25 to 0.1 AU the power rises sharply reaching 200 watts at 0.1 AU. At distances less than 0.1 AU, the increased solar input would result in excessive generator operating temperatures and a corresponding degradation of system output power. Although such a system appears unattractive from a power profile viewpoint, it is potentially useful for future solar-probe missions, such as continuous orbiting around the Sun at 0.1 AU or less.

The performance of the 0.722- and 0.388-AU systems is presented in figure 5 for

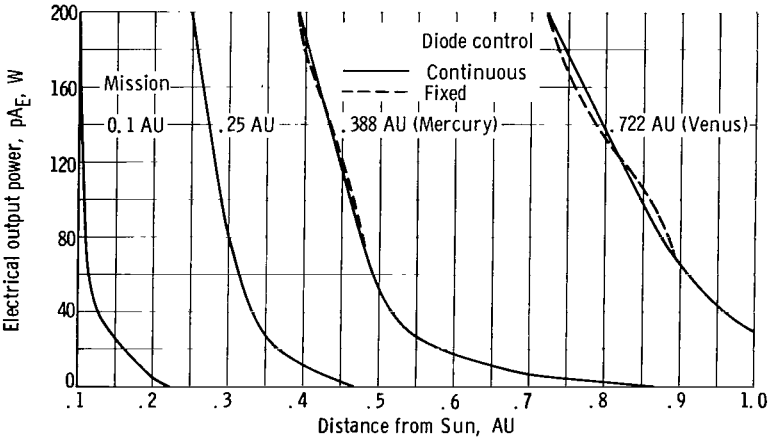

Figure 5. - Output power plotted against distance from Sun for 200-watt solar thermionic conversion systems.

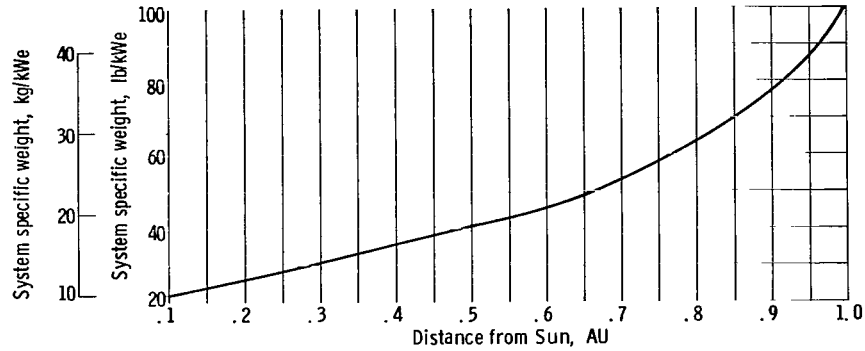

Figure 6. - Design-point system specific weight plotted against distance from Sun for 200-watt solar thermionic conversion system.

both the continuous and fixed diode control conditions (see appendix C). Note that for the 0.722-AU mission, for example, fixed diode control power output is 105 watts, while continuous diode control power is only 100 watts at 0.85 AU. This occurs because the system is designed to produce maximum output power with the thermionic converters operating at maximum diode power density rather than maximum diode efficiency. Typically, maximum diode efficiency occurs at higher values of electrode voltage than maximum power density for a given emitter temperature. (See appendix C for a further explanation.)

Design point values of thermionic system specific weight are plotted against distance from the Sun in figure 6. This specific weight decreases continuously from 100 pounds per kilowatt electric (45.4 kg/kWe) at 1.0 AU to about 22 pounds per kilowatt electric (10 kg/kWe) at 0.1 AU. Note that the specific weights presented in figure 6 represent the minimum weights determined for each design point rather than the specific weight of one particular system as a function of distance from the Sun. Thus, a solar thermionic system designed to produce 200 watts and have a specific weight of 22 pounds per kilowatt electric (10 kg/kWe) at 0.1 AU would produce very little power until the system neared the design point (fig. 5).

METHOD OF ANALYSIS FOR PHOTOVOLTAIC SYSTEM

Cell Description

A typical silicon solar cell is shown in figure 7. It consists of a silicon crystal, appropriately doped to form a p-n junction, bonded to an insulated substrate. The bottom of the crystal has a conducting coating applied for electrical interconnection. Conduction on the top is provided by a current collecting grid and a bus bar. A cover glass is placed over the cell to protect it from charged particle radiation and to improve its

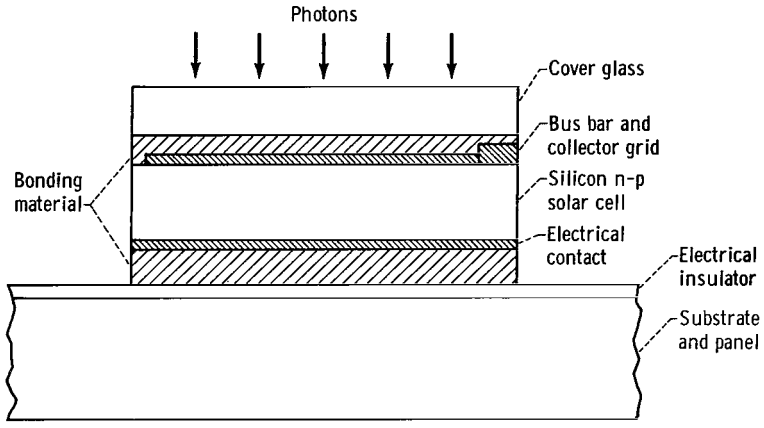

(a) Side view.

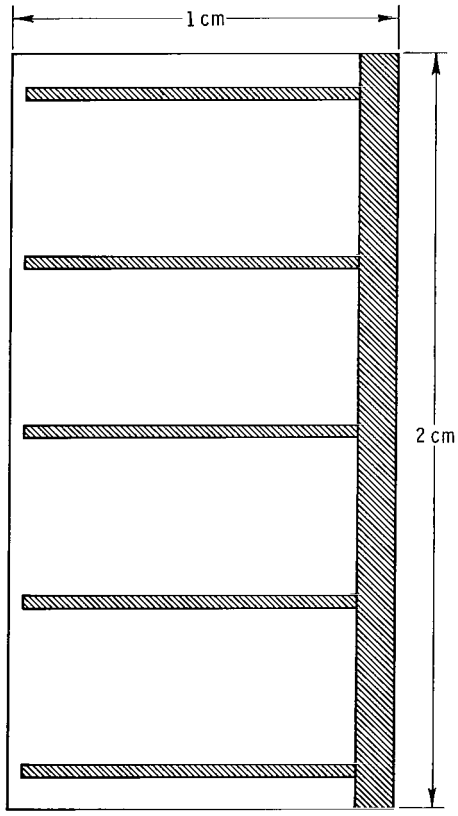

(b) Top view.

Figure 7. - Silicon solar cell.

optical properties. The thicknesses used in this study for the silicon crystal and cover glass were 13 and 6 mils, respectively. For a panel mounted array, the cells are attached to a lightweight material, such as aluminum. The panel is usually a honeycomb structure or has corrugated channeling and spars to provide added rigidity.

Thermal Analysis

The power output of a silicon solar array varies directly with the solar intensity and inversely with the cell temperature, over the temperature range of interest in this study. The cell temperature was determined by the steady-state thermal balance equation for a unit area solar array operating in space. Neglecting planetary albedo and planetary radiation input, the energy equation is

$$\underbrace{S\left[Z\alpha_o + (1 - Z)\alpha_F\right]\cos\theta}_{\text{Solar radiation input}} = \underbrace{\sigma\left[Z\epsilon_g + (1 - Z)\epsilon_F + \epsilon_B\right]T^4}_{\text{Heat radiated from cells}} + \underbrace{SZ\eta C_1\left[1 - C_2(T - 298)\right]\cos\theta}_{\text{Solar energy converted}} \tag{6}$$

This equation was solved for temperature T on a computer by using the Newton-Raphson iteration technique. The parameters and their values are defined in table II. The efficiency of the cell in air-mass-zero sunlight was taken to be 10.0 percent at 25° C (298° K). The value used for the temperature degradation coefficient C_2 was 0.46 percent per $^{\circ}$K. These values correspond to measurements on a state-of-the-art silicon cell with a resistivity of 1 ohm-centimeter (ref. 2). A factor C_1 of 0.9 was assumed for design and fabrication losses. No losses were included for power condition and radiation damage. Once the operating temperature was determined for a given point in space, the power output was computed by

$$P = SZ\eta C_1\left[1 - C_2(T - 298)\right]\cos\theta \tag{7}$$

No correction was made for the fact that the optical properties (reflection, absorption, etc.) of the cell change with the angle of incidence of the solar flux; however, an estimate of this factor was made and will be discussed in the System Performance section.

TABLE II. - PARAMETERS USED IN PHOTOVOLTAIC CALCULATIONS

Parameter	Value
Solar flux, S, W/sq ft	Depends on position in space
Packing factor, Z	0.95
Solar absorptance of cell, α_o	0.938
Solar absorptance of inactive front surface, α_F	0.10
Array tilt angle, θ, deg	Varied from 0 to 80
Stefan-Boltzmann constant, σ, W/(sq m)(^oK)	5.67×10^{-8}
Thermal emittance of glass-cell surface, ϵ_g	0.875
Thermal emittance of inactive front array surface, ϵ_F	0.90
Thermal emittance of rear array surface, ϵ_B	0.96
Temperature, T, ^oK	Depends on position in space
Efficiency of cell in air mass zero at 25° C (298 ^oK), η, percent	9.0
Design and fabrication loss factor, C_1	0.90
Efficiency degradation coefficient, C_2, percent/^oK	0.46

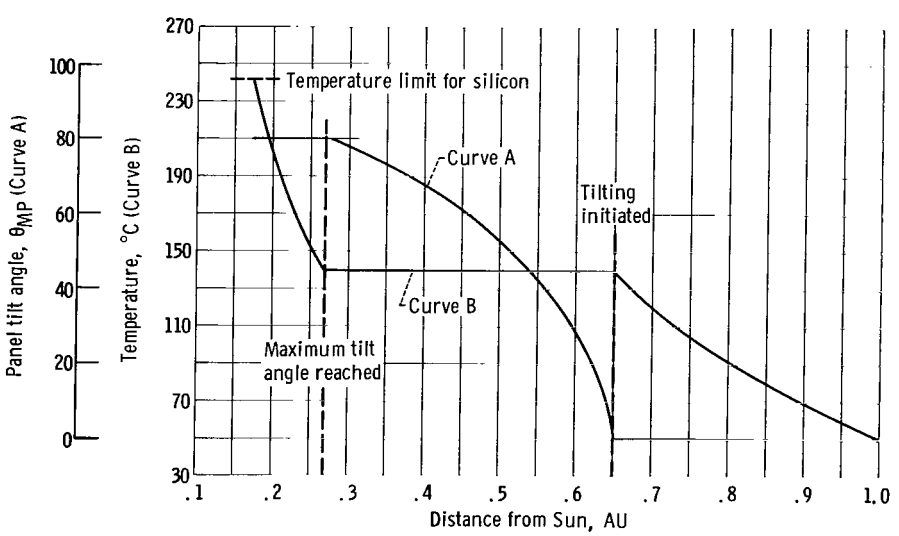

Figure 8. - Panel tilt angle and cell temperature as function of distance for silicon solar cell array.

Solar Cell Performance

The power output of an uncooled silicon cell increases with solar intensity until the point is reached where any additional power increase is offset by the decrease in cell efficiency due to a higher operating temperature. Beyond this point, if no means are provided to cool the cell, the power output drops rapidly with increasing intensity. No means were included to cool the cell directly; however, the array was tilted between 0° and 80° in order to keep the product of S cos θ at the value that produced maximum output power from the cell.

Cell temperature and θ_{MP} as a function of distance from the Sun are shown in figure 8. Here θ_{MP} is defined as the angle which the solar cell makes with the normal to the rays of the Sun at maximum power. Curve A indicates that maximum power is produced with the array normal to the rays of the Sun until a distance of 0.65 AU is reached. Beyond 0.65 AU, the cell must be tilted to maintain maximum power. At 0.27 AU, the maximum tilt angle of 80° is reached.

Curve B shows that the operating temperature of the cell increases from 51° C (324° K) at 1 AU to 135° C (408° K) at the maximum power point. After the maximum tilt angle is reached at 0.27 AU, the temperature rises rapidly as the solar flux increases. The temperature limit for silicon cells (i.e., that temperature above which power output ceases) is 242° C (515° K) based on a 10.0 percent efficient cell at 25° C (298° K) and a power degradation rate of 0.46 percent per $^{\circ}$K. Consequently, there would be no power output from a silicon array closer than approximately 0.17 AU. It should be noted that the temperature limit was based on the properties of the semiconductor material. In the experimental investigation by Johnston (ref. 3), it was found that the cell performance was limited to 190° C (463° K) mainly because of the failure of soldered contacts. This would limit the use of silicon to distances greater than 0.21 AU. However, it should be possible to develop electrical contacts that can withstand much higher temperatures.

System Performance

The power density of a silicon array is plotted against distance from the Sun in figure 9. The solid curve assumes that the incident solar flux varies with the tilt angle according to the cosine law. The power density gradually increases from 9.8 watts per square foot (105.5 W/sq m) to a maximum of 13.25 watts per square foot (142.8 W/sq m) at about 0.65 AU. This power can be maintained by tilting the array until the limiting tilt angle of 80° is reached at about 0.25 AU. Beyond 0.27 AU, the power density decreases

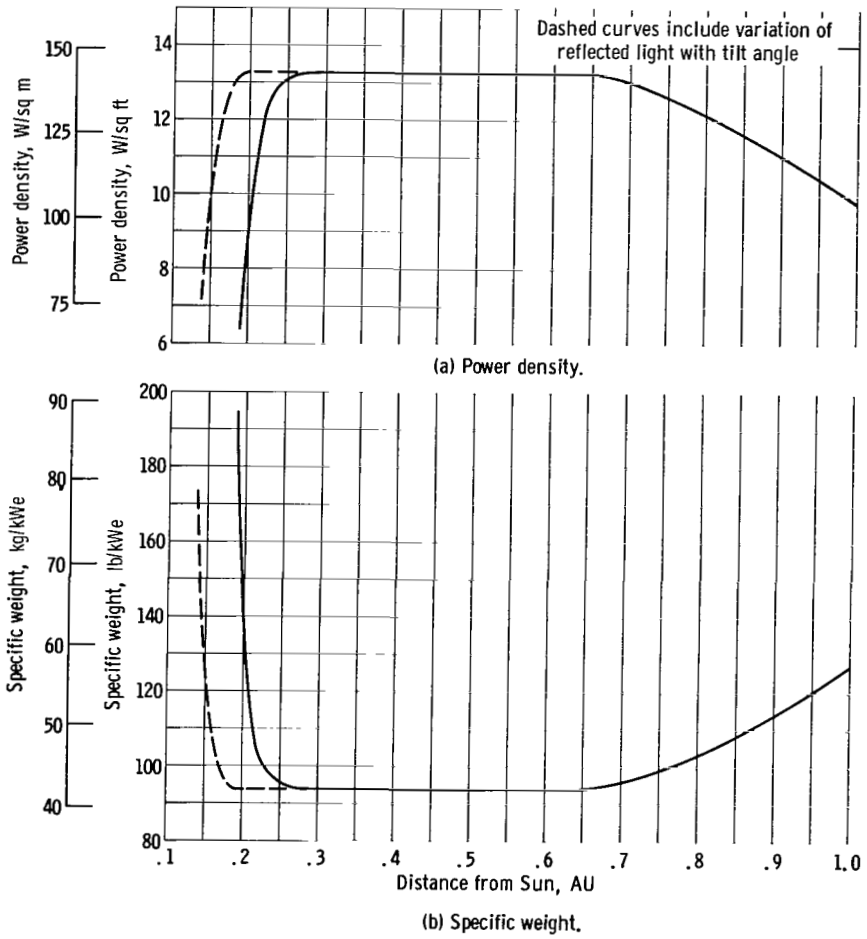

Figure 9. - Power density and specific weight plotted against distance from Sun.

rapidly as the temperature limit of the silicon cell is approached.

The dashed-line extension of the curve in figure 9(a) is an attempt to incorporate the results obtained in reference 3 into this study. Johnston determined the power output of a silicon cell for various angles of incidence. He found that the power output of the cell for constant photon flux decreased more than could be accounted for by the fact that the flux decreases as a function of the cosine of the incident angle. If it is assumed that the power output decreases because of an increase in the light reflected and that the change affects all wavelengths uniformly, a correction factor can be applied to reduce the amount of light absorbed as a function of tilt angle. This will tend to reduce the tilt angle needed to keep the solar intensity constant. Consequently, this permits a closer approach to the Sun (about 0.19 AU) before the limiting tilt angle and cell temperature are reached (fig. 9(a)).

The specific weight of a silicon solar cell array is plotted against distance from the Sun in figure 9(b). The general shape of the curve is a mirror image of the power

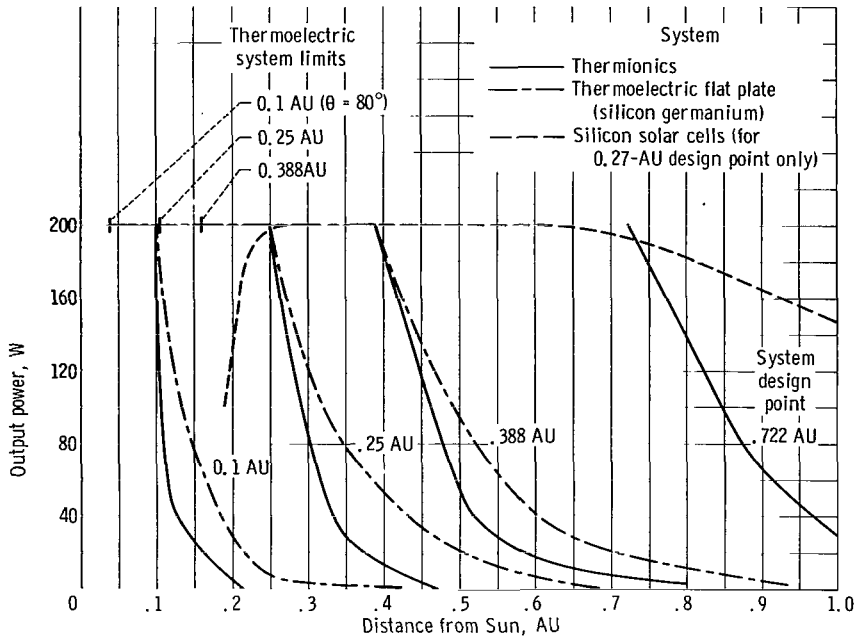

Figure 10. - Output power as function of distance from Sun for 200-watt solar conversion systems.

density curve. A constant factor of 1.25 pounds per square foot, which is within the existing state-of-the-art for silicon arrays of 1 kilowatt or less, was used to calculate the specific weight. This factor consists of 0.45 pound per square foot for the cell, cover glass, adhesives, etc., and 0.80 pound per square foot for the structure and mechanisms (i.e., hinges and springs). (No weights were included for power conditioning or orientation equipment.) The array specific weight decreases from 127.6 pounds per kilowatt (57.7 kg/kWe) at 1.0 AU to a minimum of 94.0 pounds per kilowatt (42.7 kg/kWe) at 0.65 AU. The specific weight increases rapidly with decreasing distance from the Sun after the maximum tilt angle is reached at 0.27 AU. Again, the dashed curve in figure 9(b) is based on the experimental results presented in reference 3. Advances in silicon solar cell and array technologies might reduce the specific weight of the silicon array; a substantial increase of the power per square foot of the array is less likely.

SYSTEM COMPARISONS

Power Output Comparison

The output power variation with distance is presented in figure 10 for the three conversion systems considered in this study. As seen in figure 10, only the silicon solar

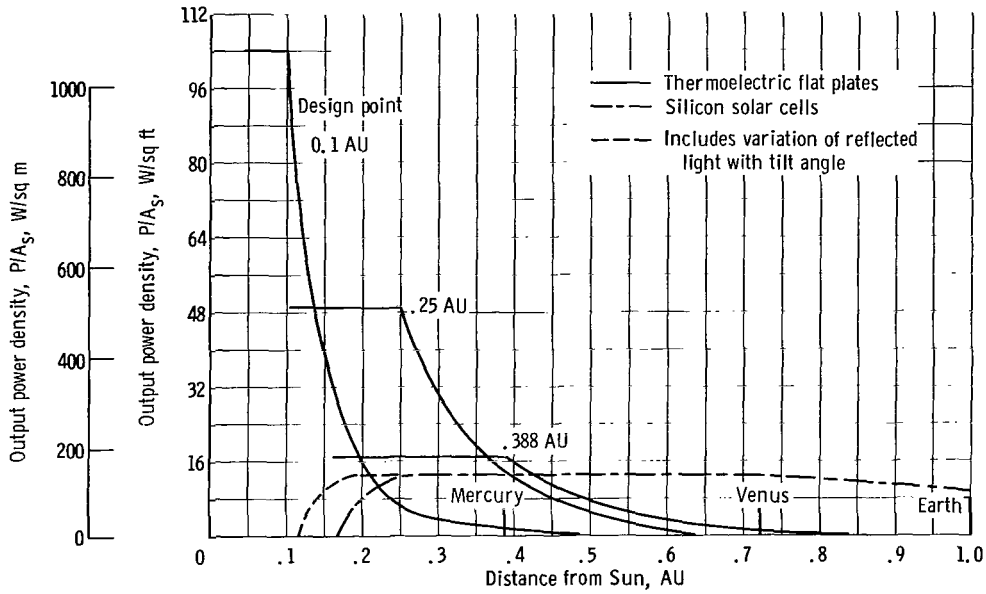

Figure 11. - Power density as function of distance from Sun for silicon-germanium thermoelectric flat plates and silicon solar cells.

cell system is capable of providing relatively constant power between 1.0 and 0.25 AU. Based on a maximum output power of 200 watts, the solar cell array provides from 146 watts at 1.0 AU to 200 watts from 0.6 to 0.27 AU.

The thermionic and thermoelectric systems, being dependent on thermal power density, exhibit a behavior similar to the variation of solar flux with distance (see fig. 10). A thermionic system designed to produce 200 watts at 0.1 AU, for example, provides no power at 1.0 AU and only 26 watts at 0.15 AU, while a corresponding thermo electric system exhibits a similar power profile but slightly higher power, providing about 75 watts at 0.15 AU. In addition, the thermoelectric flat-plate operation can be extended from 0.1 to 0.04 AU by tilting the plate to a maximum angle of 80°.

The power density variation with distance for the thermoelectric and solar cell panels is presented in figure 11. Note that the thermoelectric power density at 0.1 AU (104 W/ft^2) (1120 W/sq m) is almost eight times that of solar cells (13.3 W/ft^2) (143.2 W/sq m), which suggests that the addition of a relatively small thermoelectric panel to a solar cell array would yield a hybrid system capable of providing constant power output from Earth to 0.1 AU or less. The specific weight of such a hybrid system is discussed in the following section.

Specific Weight Comparison

A plot of design-point-system specific weight against distance is presented in

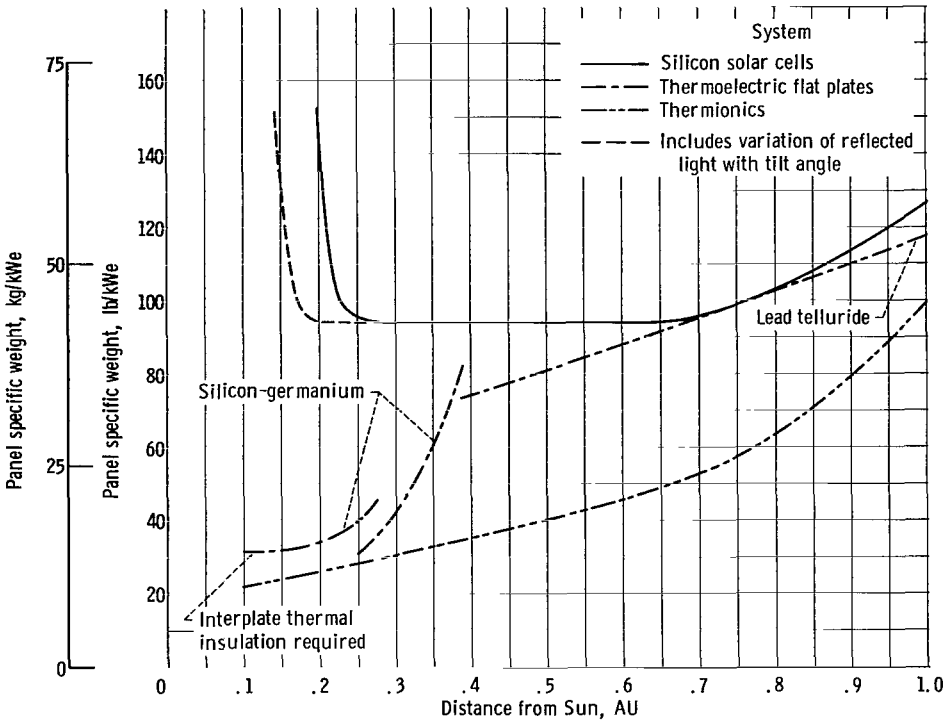

Figure 12. - Specific weight as function of distance from Sun for three systems studied.

figure 12 for the three conversion systems. Silicon solar cell specific weight minimizes at about 94 pounds per kilowatt electric (44.5 kg/kWe) between 0.65 and 0.27 AU, while thermoelectric and thermionic weights of between 20 and 30 pounds per kilowatt electric (9.1 and 13.6 kg/kWe) are indicated between 0.25 and 0.1 AU.

The specific weight of a hybrid system of solar cells and thermoelectric panels would be the sum of the individual specific weights. Thus, for a 0.1-AU mission, a silicon solar cell array combined with a thermoelectric flat plate utilizing silicon-germanium semiconductors results in a total system specific weight of 22 plus 94, or 116 pounds per kilowatt electric (52.6 kg/kWe).

SUMMARY OF RESULTS

A study of the solar direct-energy conversion systems operating between 1.0 and 0.1 AU yielded the following results:

1. Of the three systems considered, silicon solar cells provide the best overall power profile from 1.0 to 0.25 AU; however, if no active cooling and a maximum tilt angle of 80^{o} are assumed, output power drops off sharply at distances less than about 0.2 AU and falls to zero between 0.2 and 0.15 AU because of excessive cell operating temperatures.

2. Thermionic and thermoelectric systems could be designed to operate at 0.1 AU or closer; however, extreme output power variations would be encountered during flight.

3. All three systems exhibited specific weights on the order of 100 pounds per kilowatt electric (45.4 kg/kWe) or less in the 1.0- to 0.2-AU range; therefore, the system specific weight is not considered an important basis of comparison in this range. However, at distances less than about 0.2 AU, where the silicon array no longer produces power, thermionic and thermoelectric system specific weights of less than 40 pounds per kilowatt electric (18.1 kg/kWe) are indicated.

4. Silicon solar cells and silicon-germanium flat plates were compared on the basis of output power density. The power density for the silicon-germanium flat plate (50 to 100 W/ft^2) (539 to 1077 W/sq m) in the range 0.25 to 0.4 AU is four to eight times that of solar cells (13.3 W/ft^2) (143 W/sq m) at 0.25 AU. The preceding fact suggests the use of a hybrid system for a solar-probe mission using, for example, 15 square feet of solar cell panels and 2 to 4 square feet of silicon-germanium flat plates to provide a continuous power output of a few hundred watts from 1.0 to 0.1 AU.

Lewis Research Center,
National Aeronautics and Space Administration,
Cleveland, Ohio, August 4, 1966,
120-27-06-06-22.

APPENDIX A

SYMBOLS

A	area, sq ft, sq m, sq cm
C_1	design and fabrication loss factor
C_2	efficiency degradation coefficient, percent/^{o}K
ℓ	thermoelectric element length, in.
P	electrical power, W
p	power density, W/cm^2
Q	thermal power, W
R	resistance, Ω
r	reflectance
S	solar flux, W/ft^2
T	temperature, ^{o}F or ^{o}K
Z	packing factor
α	solar absorptance
ϵ	thermal emittance
η	efficiency, percent
θ	array tilt angle, deg
σ	Stefan-Boltzmann constant, W/(m^2)(^{o}K)
φ	rim angle, deg

Subscripts:

a	absorber
B	rear array surface
C	cold junction
C-A	collector-absorber
Cs	cesium reservoir
c	thermoelectric cross section
d	device
E	emitter
F	inactive front array surface
g	glass-cell surface
H	hot junction
i	interplate losses
L	load
MP	maximum power
m	mica supports
O	overall
o	cell
r	radiator
s	surface of absorber

APPENDIX B

SPECIFIC SYSTEM DESCRIPTION AND DEVICE PERFORMANCE FOR THERMOELECTRIC FLAT PLATE

Two different semiconductor materials are considered for the flat-plate thermoelectric generator: lead telluride and silicon germanium. Cylindrical thermoelectric elements 0.1-inch (2.54 mm) in diameter and 0.2-inch (5.08 mm) long are assumed. Five-mil- (0.127 mm) thick rigid plates are assumed for both absorber and radiator. Four 0.4- (10.16 mm) by 0.2- (5.08 mm) by 0.001-inch (0.0254 mm) thin mica support sheets are included per thermocouple.

Device power density P/A_c and device efficiency η_d calculations were made by using the equations presented in reference 4 for a range of hot- and cold-junction temperatures. The device power density is defined as the electrical power produced per unit of thermoelectric cross-sectional area. Device efficiency is defined as the ratio of the electrical output power to the thermal input power delivered to the thermoelectric device. Both device power density and efficiency, which are presented for lead telluride and silicon germanium in figure 13, are based on the assumption that the electrical lead resistance is equal to 10 percent of the thermoelement resistance and that the electrical contact resistance per junction is approximately 2 percent of the thermoelement resistance. (The electrical contact resistance is the resistance of the junction interface between the thermoelectric element and either the absorber or the radiator plate, as shown in fig. 14.) For a given hot-junction temperature T_H, both thermoelectric device power density and efficiency increase with decreasing cold-junction temperature. For example, as shown in figure 13(a), at a hot-junction temperature of 1000° F (811° K) and a cold-junction temperature of 700° F (644° K), the lead telluride device power density and efficiency are 162 watts per square foot (1745 W/sq m) and 3.15 percent, respectively. When the cold-junction temperature is reduced to 500° F (533° K), P/A_c and η_d are increased to 530 watts per square foot (5710 W/sq m) and 5.3 percent, respectively. Figure 13(b) shows a similar behavior for silicon germanium, where, for example, at a hot-junction temperature of 1800° F (1255° K), the device power density and efficiency increase, respectively, from 1480 watts per square foot (15 940 W/sq m) and 4.3 percent at a cold-junction temperature of 1100° F (866° K) to 3170 watts per square foot (34 200 W/sq m) and 6.2 percent at a cold-junction temperature of 800° F (700° K).

For the lead telluride system, the absorber and radiator plates are assumed to serve as the electrical leads, while for the silicon-germanium system, stack-type

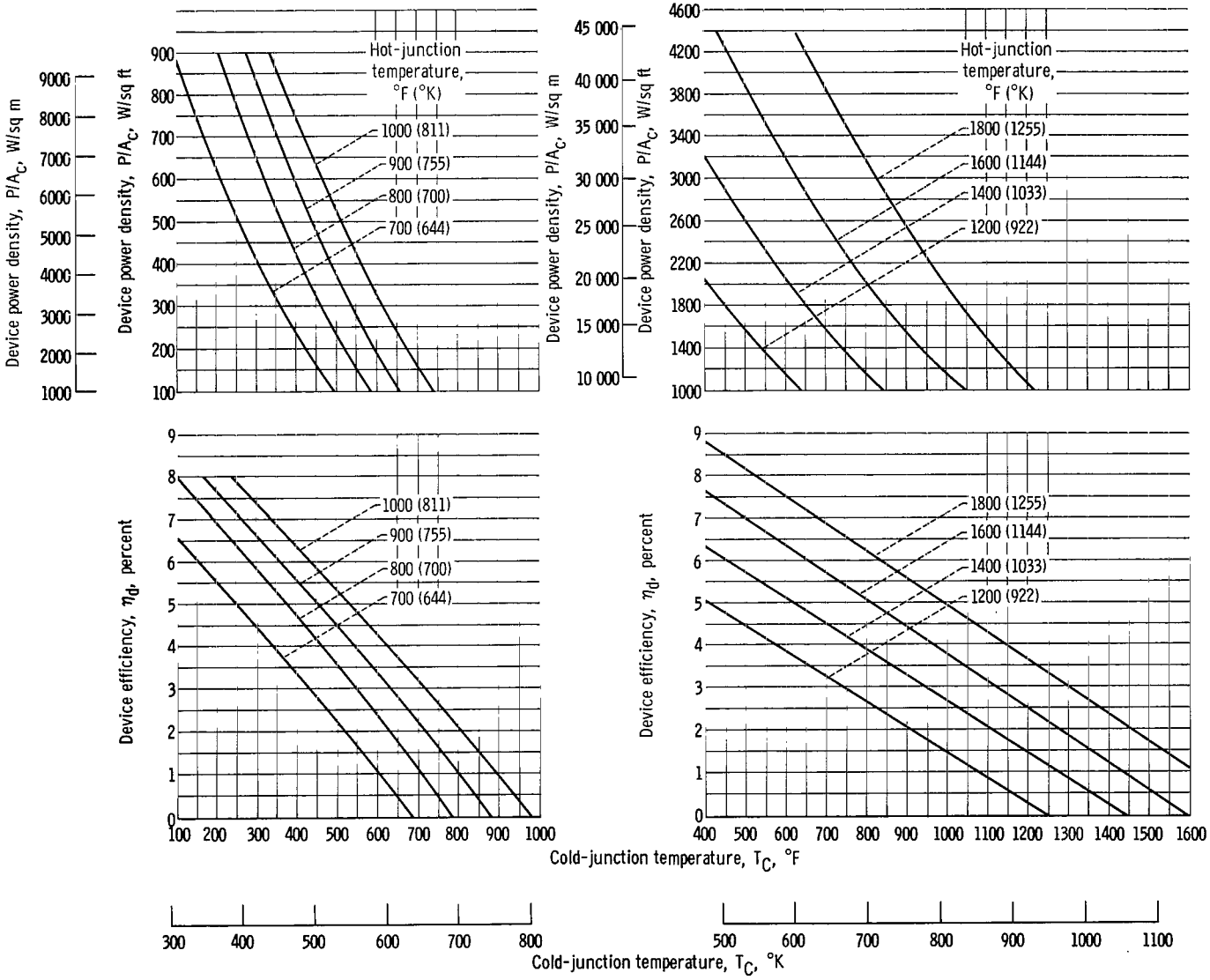

Figure 13. - Device power density and efficiency plotted against cold-junction temperature for lead telluride and silicon-germanium semiconductors. Thermoelectric element length, 0.2 inch.

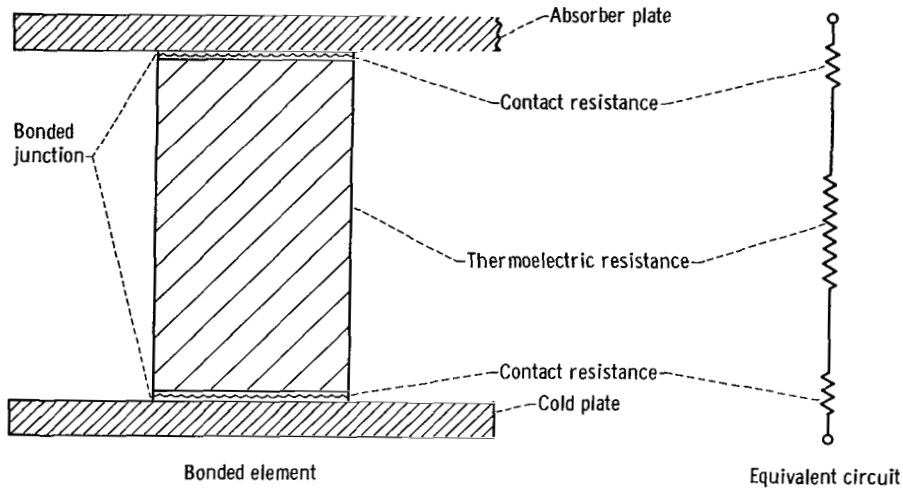

Figure 14. - Effective resistance of bonded thermoelectric element.

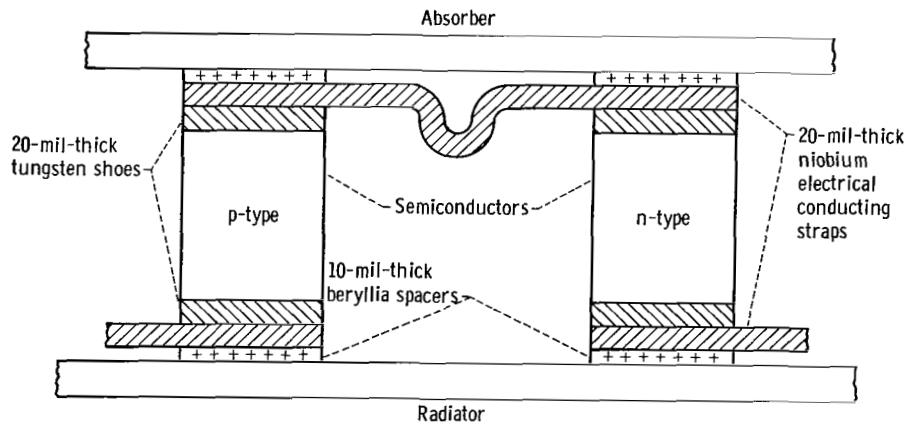

Figure 15. - Stack-type interconnections assumed for silicon-germanium flat-plate generator.

interconnections are used as follows (see fig. 15): at the end of each element, a 0.020-inch-thick (0.508 mm) tungsten shoe is bonded to the silicon-germanium semiconductor. A 0.020-inch-thick (0.508 mm) niobium electrical conducting strap is used to connect adjacent elements, and 0.010-inch-thick (0.254 mm) beryllia spacers electrically insulate the elements from the absorber and radiator plates.

APPENDIX C

THERMIONIC SYSTEM

Specific System Description and Component Performance

Thermionic diode performance for this study is based on a rhenium-emitter - molybdenum-collector diode with a 3-mil (0.0761 mm) interelectrode spacing (ref. 5). Diode power density and efficiency are plotted against emitter temperature for this converter in figure 16. The power density is obtained directly from reference 5; however, since the corresponding diode efficiency is not presented in this reference, the efficiencies were calculated by using an energy balance approach. Two curves are presented for both power density and efficiency in figure 16; one represents diode performance obtained by continuous adjustment of the cesium reservoir temperature T_{Cs} and the load resistance R_L, and the second represents the performance obtained by fixing T_{Cs} and R_L at the required optimum values for an emitter temperature of 2050° K. The first case will be referred to as "continuous diode control" and the second as "fixed diode control."

As shown in figure 16, the diode power density and calculated efficiency for the continuous diode control case vary from 20.8 watts per square centimeter and 14.8 percent at an emitter temperature T_E of 2050° K to 10.4 watts per square centimeter and 10.3 percent at $T_E = 1850^{\circ}$ K. For the fixed diode control case, the cesium reservoir temperature and load resistance are fixed at 643° K and $0.0181/A_E$ ohm, respectively, where A_E is the diode emitter area in square centimeters. The diode power density and calculated efficiency for the fixed diode control case vary from 20.8 watts per square centimeter and 14.8 percent at $T_E = 2050^{\circ}$ K to 7.5 watts per square centimeter and 9 percent at $T_E = 1850^{\circ}$ K.

In the discussion of thermionic system performance, it was pointed out that fixed diode control results, in some cases, in greater output power than continuous diode control. As shown in figure 16(c), for emitter temperatures less than 1980° K, more thermal power is required by the converters to operate at a given emitter temperature with continuous diode control than with fixed diode control. For example, at an emitter thermal input power density of 105 watts per square centimeter, the continuous diode control results in an emitter temperature of 1880° K and a power density (fig. 16(a)) of 11.8 watts per square centimeter, while fixed diode control results in an emitter temperature of 1925° K and a power density of 12.0 watts per square centimeter. Thus, for the 0.722-AU system (see fig. 5) a more efficient utilization of thermal energy is effected at 0.85 AU with the fixed diode control condition, and hence operation at a higher emitter temperature. In this case then, little or no advantage is gained from continuous diode control.

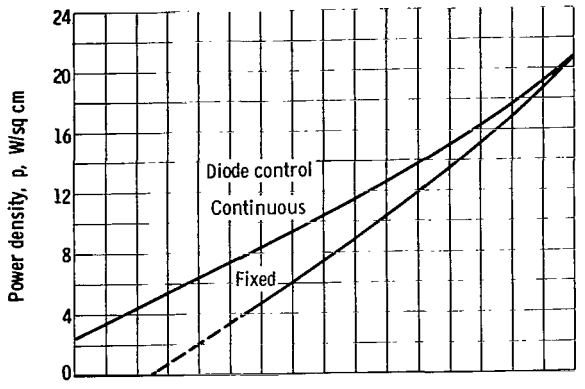

(a) Power density.

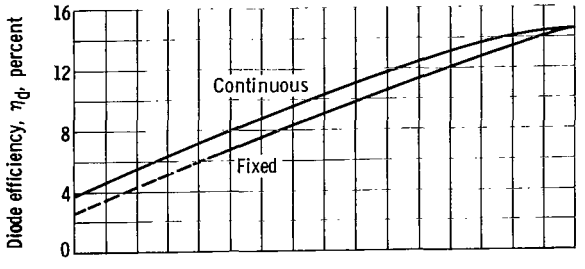

(b) Diode efficiency.

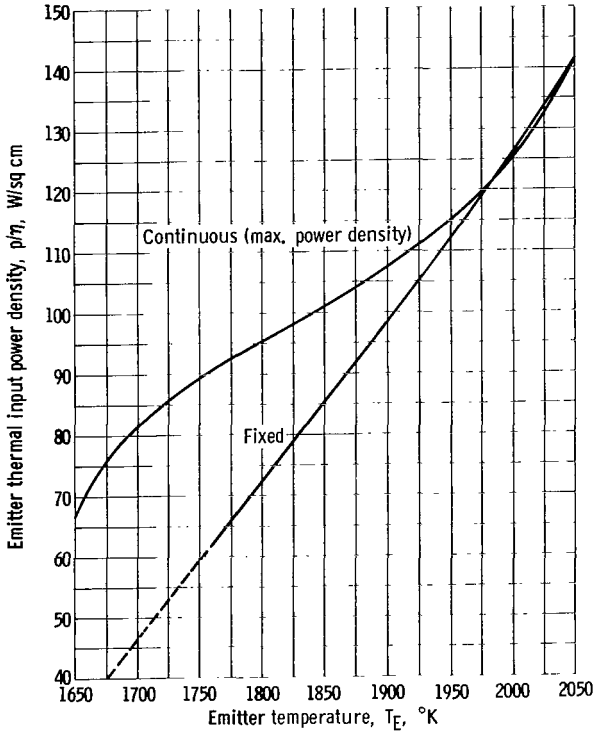

(c) Thermal input power density.

Figure 16. - Power density, diode efficiency, and thermal input power density plotted against emitter temperature for rhenium-molybdenum diode with interelectrode spacing of 3 mils (0.0762 mm). (Dashed parts of curves denote extrapolation.)

Collector-Absorber Performance

Solar collector-absorber performance is calculated for a perfectly oriented parabolic collector having a diameter of 5 feet, a rim angle φ of 60°, a reflectivity r of 0.9, and a normal distribution of collector surface errors with a standard deviation σ of 6 minutes. Five percent of the collector projected area is assumed obscured by the generator and its supports. Initially, a digital computer program is used to predict the maximum collector-absorber efficiency as a function of distance from the Sun by assuming a cavity having blackbody characteristics and a cavity temperature of 2050° K. Corrections are then included for reflection and reradiation of energy from the generator aperture by using the approach outlined in reference 6 and by assuming an appropriately sized generator having a cavity length-to-width ratio of 2 and an inner-wall emittance of 0.5. The corrected collector-absorber efficiency as a function of distance from the Sun is plotted in figure 17. Note the sharp decrease in collector-absorber efficiency for distances less than 0.3 AU. Because of the increased size of the image of the Sun in this region, the solar energy directed into the aperture of the generator is focused less sharply so that relatively large aperture areas are necessary. The increased thermal losses from the aperture thus result in a reduction in collector-absorber efficiency. (It is important to realize that fig. 17 represents the performance of a collector-absorber system with a variable aperture; i.e., each point

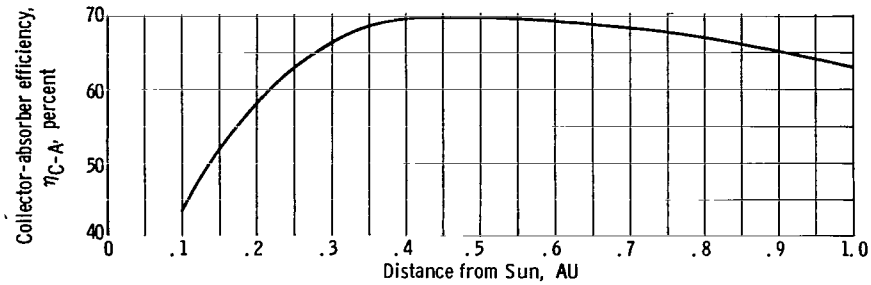

Figure 17. - Maximum collector-absorber efficiency plotted against distance from Sun for cavity temperature of 2050° K.

on the abscissa of fig. 17 represents a different optimum aperture size.)

The effect of misorientation of the solar concentrator was determined for the 1.0-AU design point only. It was found that a misorientation angle of approximately 10 minutes results in a 10-percent reduction in output power at design point. For distances less than 1.0 AU, the effect of misorientation is expected to decrease since the solar energy focused into the generator is less sharply defined (i.e., because of the divergence angle of the rays of the Sun, the collector focusing ability decreases as the system approaches the Sun).

Lightweight aluminum solar concentrators proposed for Earth orbital missions are not suitable for the higher temperatures encountered by solar probes. For purposes of calculating system weight, the typical weight estimate of 0.6 pound per square foot for 1.0-AU missions was increased to 1.0 pound per square foot for 0.722-, 0.388-, 0.25-, and 0.1-AU missions.

The thermionic converter specific weight (including the radiator) is scaled linearly from the solar energy thermionic system diode weight (i.e., 0.22 lb/cm^2 of emitter area) presented in reference 7. The generator support structure is taken as 0.25 of the collector weight.

The thermal shields are considered to be thin parallel plates arranged such that the heat transfer between shields is due solely to radiation. Weight calculations are based on the use of 0.3-mil-thick tantalum shields having an emissivity of 0.3.

REFERENCES

1. Lieblein, Seymour: Analysis of Temperature Distribution and Radiant Heat Transfer Along a Rectangular Fin of Constant Thickness. NASA TN D-196, 1959.
2. Broder, Jacob D.; Kautz, Harold E.; Mandelkorn, Joseph; Schwartz, Lawrence; and Ulman, Robert P.: Solar-Cell Performance at High Temperatures. NASA TN D-2529, 1964.
3. Johnston, Phillip A.: Laboratory Experiments on the Performance of Silicon Solar Cells at High Solar Intensities and Temperature. NASA TN D-2733, 1965.
4. Cadoff, Irving B.; and Miller, Edward, eds.: Thermoelectric Materials and Devices. Reinhold Publishing Corp., 1960.
5. Kitrilakis, S. S.; and Weinstein, J. H.: Thermionic Emitter Materials Research Program. Rep. No. 27-64, Thermo Electron Engineering Corp., 1963. (Available from DDC as AD-425895.)
6. Stephens, Charles W.; and Haire, Alan M.: Internal Design Considerations for Cavity-Type Solar Absorbers. ARS J. vol. 31, no. 7, July 1961, pp. 896-901.
7. Menetrey, W. R.; and Smith, A.: Solar Energy Thermionic Conversion System. Paper No. 2499-62, ARS, Sept. 1962.

"The aeronautical and space activities of the United States shall be conducted so as to contribute . . . to the expansion of human knowledge of phenomena in the atmosphere and space. The Administration shall provide for the widest practicable and appropriate dissemination of information concerning its activities and the results thereof."

—NATIONAL AERONAUTICS AND SPACE ACT OF 1958

NASA SCIENTIFIC AND TECHNICAL PUBLICATIONS

TECHNICAL REPORTS: Scientific and technical information considered important, complete, and a lasting contribution to existing knowledge.

TECHNICAL NOTES: Information less broad in scope but nevertheless of importance as a contribution to existing knowledge.

TECHNICAL MEMORANDUMS: Information receiving limited distribution because of preliminary data, security classification, or other reasons.

CONTRACTOR REPORTS: Technical information generated in connection with a NASA contract or grant and released under NASA auspices.

TECHNICAL TRANSLATIONS: Information published in a foreign language considered to merit NASA distribution in English.

TECHNICAL REPRINTS: Information derived from NASA activities and initially published in the form of journal articles.

SPECIAL PUBLICATIONS: Information derived from or of value to NASA activities but not necessarily reporting the results of individual NASA-programmed scientific efforts. Publications include conference proceedings, monographs, data compilations, handbooks, sourcebooks, and special bibliographies.

Details on the availability of these publications may be obtained from:

SCIENTIFIC AND TECHNICAL INFORMATION DIVISION

NATIONAL AERONAUTICS AND SPACE ADMINISTRATION

Washington, D.C. 20546